SLAC–PUB–7156
April 1996

STRUCTURED TARGETS AND THE LANDAU-POMERANCHUK-MIGDAL EFFECT *

Richard Blankenbecler

Stanford Linear Accelerator Center
Stanford University, Stanford, California 94309
e-mail: rzbth@slac.stanford.edu

Abstract

The Landau-Pomeranchuk-Migdal effect is the suppression of Bethe-Heitler radiation caused by multiple scattering in the target medium. In this paper, the quantum treatment given earlier for finite but homogeneous targets is extended to structured targets. It is shown that radiators composed of separated plates or of a medium with a varying radiation length can exhibit coherence maxima and minima in their photon spectra.

Submitted to *Physical Review D.*

*Work supported by the Department of Energy, contract DE–AC03–76SF00515.

1 Introduction and Motivation

In a previous paper[1] by S. D. Drell and the author, a quantum treatment of the bremsstrahlung of photons by a charged particle undergoing random multiple scattering was given. This treatment included as limiting cases the familiar Bethe-Heitler (BH) radiation[2] from a charged particle scattering from an isolated atom relevant for a thin target, and in the opposite limit the Landau-Pomeranchuk[3]-Migdal[4] (LPM) effect which has been experimentally verified[5] to suppress the radiation for a thick target. This formulation included the effects of a finite target thickness in such a way as to smoothly connect these two limits.

In reference[1] , eikonal techniques developed earlier to treat the beamstrahlung process[6] in colliding beams were applied to the problem of radiation in a scattering medium. This approach lead to a physically clear quantum mechanical treatment of multiple scattering and then to a derivation of the LPM suppression of soft photon radiation from high energy electrons in matter.

This suppression effect was first described by Landau and Pomeranchuk[3] who treated the classical radiation of a high energy particle in the fluctuating and 'random' field inside an infinitely thick medium. Subsequently Migdal[4] presented a quantum mechanical derivation of this effect, treating multiple scattering via the Vlasov equation and including the effects of electron spin and energy loss.

The physics of the LPM effect is that of the formation length of the photon given by $l_f = 2pp'/(m^2 k)$. This is the path length required by the uncertainty relation for a high energy electron of initial momentum p, final momentum p', and mass m, to radiate a photon of momentum k near the forward direction. At high energies ($p,\ p' >> m$) and for soft photon emission $k << p$, the formation length l_f can grow quite large relative to the scattering mean free path of the electron, eventually

becoming macroscopic. When this occurs, there is a loss of coherence during the emission of the photon that leads to suppression in spite of the net increase in the amount of acceleration of the charge.

There have been many papers which extended the classical treatment of the LPM effect including [7], [8], and [9] in which certain errors in the original derivation are corrected. A general and clear treatment of semiclassical photon radiation can be found in the review paper by A.I. Akhiezer and N. F. Shul'ga[10]. A more accurate treatment of the coulomb nature of the basic scattering process has recently been given[11] for an infinite target.

2 Eikonal Treatment

We review here the eikonal formulation for high energy scattering by the static fields of a medium at rest; for more details, see Ref. [1]. For simplicity we first consider the Klein-Gordon equation for a scalar particle of mass m in a static external field, which can be written

$$[(E-V)^2 + \overrightarrow{\bigtriangledown}^2 - m^2]\phi(\overrightarrow{r}) = 0 \ . \tag{1}$$

We look for solutions satisfying the requisite initial and final (outgoing and incoming) boundary conditions and write

$$\phi(\overrightarrow{r}) \ = \ \exp(i\Phi(\overrightarrow{r})) \ , \tag{2}$$

where the phase function Φ satisfies the equation

$$(E-V)^2 - m^2 \ = (\overrightarrow{\bigtriangledown}\Phi(\overrightarrow{r}))^2 - i\overrightarrow{\bigtriangledown}^2\Phi(\overrightarrow{r}) \ . \tag{3}$$

For the incident wave with its outing wave boundary conditions, the leading term in Φ_i will be $p^i z$ corresponding to the incident particle momentum along the z-axis.

For the final state with incoming wave boundary conditions, the leading term in Φ_f must contain the final electron momentum written as $\overrightarrow{p}^f = (\overrightarrow{z}p^f + \overrightarrow{b}p_\perp^f)$. In order to properly include the 'bending' of the wave, the phase functions must be determined to order $(1/p)$. Thus one writes schematically

$$\Phi^{i,f} = \overrightarrow{p}^{i,f} \cdot \overrightarrow{r} - \chi_0^{i,f}(z, \overrightarrow{b}_\perp) - \frac{1}{p^{i,f}} \chi_1^{i,f}(z, \overrightarrow{b}_\perp) . \tag{4}$$

Substitution into Eq.3 then yields the solutions exhibited in Ref. [1].

The total phase appearing in the bremsstrahlung matrix element, also includes the phase of the photon wave function $A(\overrightarrow{r})$. Defining the momentum transfer to the medium as $\overrightarrow{q} = \overrightarrow{p}^f + \overrightarrow{k} - \overrightarrow{p}^i$, the total phase can be written in the form

$$\begin{aligned} \Phi^{\rm tot} &= \Phi^i - \Phi^f - \overrightarrow{k} \cdot \overrightarrow{r} \\ &= -\overrightarrow{q} \cdot \overrightarrow{r} - \chi_0^{\rm tot}(\overrightarrow{b}_\perp) - \frac{1}{p} \chi_1^{\rm tot}(z, \overrightarrow{b}_\perp) , \end{aligned} \tag{5}$$

where from now on $p \equiv p^i$ and total phase functions have been introduced as the appropriate sum of a χ and a τ. Therefore the zeroth order term is independent of z

$$\chi_0^{\rm tot}(\overrightarrow{b}_\perp) = \int_{-\infty}^{\infty} dz' V(z', \overrightarrow{b}_\perp) , \tag{6}$$

while the first order terms, given explicitly in Ref.[1], still retain some z-dependence. These first order terms, which reflect the bending of the particle trajectory, involve quantities of the form:

$$\begin{aligned} \overrightarrow{A}_\perp(z_2, z_1) &= \int_{z_1}^{z_2} dz' \overrightarrow{E}_\perp(z') \\ \int_{z_1}^{z_2} dz \overrightarrow{A}_\perp(z, z_1) &= \int_{z_1}^{z_2} dz' \overrightarrow{E}_\perp(z') (z_2 - z') . \end{aligned} \tag{7}$$

The integral $\overrightarrow{A}_\perp(z_2, z_1)$ evidently represents the total transverse momentum accumulated in going from the point z_1 to the point z_2 in the target.

The matrix element for single photon emission was discussed using the above approximations and the final probability for emission was evaluated. The final result for a given field distribution in the target was given in Ref.[1] in the form

$$\frac{\pi(1-x)}{\alpha x}\,\frac{dP(x)}{dx} \;=\; I \;=\; \int_{-\infty}^{\infty} db_2 \int_{-\infty}^{b_2} db_1\, I(b_2,b_1,b_l)\;, \tag{8}$$

where

$$\begin{aligned} I(b_2,b_1,b_l) &= 2\,\frac{C(b_2)C(b_1)}{b}\left\{[1+\frac{1}{2}r(x)\lambda(b_2,b_1,b_l)]\,\sin(c)-\sin(b)\right\}\;, \\ c &= b\,[\,1+\eta(b_2,b_1,b_l)\,]\;, \end{aligned} \tag{9}$$

and the dimensionless variables are defined by $b_i = z_i/l_f$ and $b = b_2 - b_1$.

The field dependent quantities $\lambda(z_2,z_1,l)$ and $\eta(z_2,z_1,l)$ are given by

$$z^2\,m^2\,\eta(z_2,z_1,l) \;=\; z\int_{z_1}^{z_2} dz[\,\overrightarrow{A}_\perp(z,z_1)]^2 - [\int_{z_1}^{z_2} dz\,\overrightarrow{A}_\perp(z,z_1)\,]^2\,, \tag{10}$$

$$m^2\,\lambda(z_2,z_1,l) \;=\; [\,\overrightarrow{A}_\perp(z_2,z_1)]^2\;, \tag{11}$$

where $z = z_2 - z_1$.

3 Statistical Averages for a Structured Target

The model introduced in Ref.[1] reflects the fact that each incident electron experiences a very different arrangement of the atomic electric fields. The statistical average involved is therefore the average over the wave packets of the individual electrons. As noted before, the $1/p$ terms in the eikonal phase record the transverse momenta transferred to the incoming and outgoing particle and depend only on the penetration depth z . Therefore for this non-crystalline medium we set

$$V(z,\,\overrightarrow{b}_\perp) \;=\; -\,\overrightarrow{b}_\perp \cdot \overrightarrow{E}_\perp(z)\;. \tag{12}$$

The transverse field varies with depth z from atomic layer to atomic layer. The quantity $\overrightarrow{E}_{\perp}(z)\,dz$ is simply the differential transverse momentum acquired in traversing the medium from z to $z+dz$. Its statistical average is given by

$$\left\langle \overrightarrow{E}_{\perp}(z_2)\cdot\overrightarrow{E}_{\perp}(z_1)\right\rangle \;=\; \frac{<\overrightarrow{p}_{\perp}^{\,2}>}{L(z_2)}\,\delta(z_2-z_1)\;. \tag{13}$$

where explicit note has been taken that the medium may vary from layer to layer so that the radiation length depends upon position. This relation allows one to compute all statistical averages that will be needed. Note that the average transverse momentum accumulated via multiple scattering in traversing one radiation length of target is given by $<\overrightarrow{p}_{\perp}^{\,2}>=\,2\pi m^2/\alpha$.

The main formulae that we will need all arise from noting that the transverse electric field is zero outside the region $0<z<l$ where l is the total thickness of the target. The statistical averages for the needed quantities can be computed directly from the above and from formulae given in Ref.[1]. Using Eq. 7, one finds in terms of the scaled variables that

$$\langle\lambda(b_2,b_1,b_l)\rangle \;=\; l_f\,\frac{2\pi}{\alpha}\int_{b_1}^{b_2}\frac{db'}{L(b')} \tag{14}$$

$$\langle\eta(b_2,b_1,b_l)\rangle \;=\; l_f\,\frac{2\pi}{\alpha}\int_{b_1}^{b_2}\frac{db'}{L(b')}\frac{(b_2-b')(b'-b_1)}{b^2}\;, \tag{15}$$

where $b=b_2-b_1$. $L(z)$ is the radiation length that is taken to be infinite outside the target, i.e., for $z<0.0$ and for $z>l$. Recognizing αL as the mean free path, it is convenient to introduce the thickness of the target in units of the average inverse mean free path as

$$T \;=\; l_f\,\frac{\pi}{3\alpha}\int_0^{b_l}\frac{db'}{L(b')} \;=\; \frac{\pi}{3\alpha}\int_0^{l}\frac{dz'}{L(z')}\;. \tag{16}$$

This allows the overall scales to be extracted from λ and η. To this end define

$$\langle\lambda(b_2,b_1,b_l)\rangle \;=\; 6\,T\,\bar{\lambda}(b_2,b_1,b_l) \tag{17}$$

$$\langle\eta(b_2,b_1,b_l)\rangle \;=\; 6\,T\,\bar{\eta}(b_2,b_1,b_l)\;, \tag{18}$$

where

$$\bar{\lambda}(b_2, b_1, b_l) = \int_{b_1}^{b_2} \frac{db'}{L(b')} \Big/ \int_0^{b_l} \frac{db'}{L(b')} \tag{19}$$

$$\bar{\eta}(b_2, b_1, b_l) = \int_{b_1}^{b_2} \frac{db'}{L(b')} \frac{(b_2 - b')(b' - b_1)}{b^2} \Big/ \int_0^{b_l} \frac{db'}{L(b')} \ . \tag{20}$$

The explicit statistical averages for a homogeneous target plate of thickness l are readily evaluated. The results for b_2 and b_1 in the regions before, inside, and after the target, denoted by $(-\,,0\,,+)$ respectively, are

Region $(b_2\, b_1)$	$6\ b_l\ b^2\ \bar{\eta}(b_2, b_1, b_l)$	$\lambda(b_2, b_1, b_l)$
$(-\ -)$	0	0
$(0\ -)$	$b_2^2\,[3b - 2b_2]$	b_2/b_l
$(+\ -)$	$b_l\,[3(b_2 + b_1)b_l - 2b_l^2 - 6b_1 b_2]$	1
$(0\ \ 0)$	b^3	b/b_l
$(+\ 0)$	$(b_l - b_1)^2\,[3b - 2(b_l - b_1)]$	$(b_l - b_1)/b_l$
$(+\ +)$	0	0

These formulas join smoothly at all common boundaries of the regions. In addition, the symmetry between $(+)$ and $(-)$, that is $(b_2 \leftrightarrow b_l - b_1)$, is also evident.

4 Emission Probability

In Ref.[1], the statistical average of the probability of emission was evaluated in the LPM approximation, which simply replaces the field quantities $\lambda(b_2, b_1, b_l)$ and $\eta(b_2, b_1, b_l)$ by their averages. This approximation is not necessary, as will be shown in a subsequent paper[13], but is convenient and straightforward. Eliminating the integration variable b_1 in favor of b yields

$$\frac{\pi(1-x)}{\alpha x} \frac{dP(x)}{dx} = < I > = \int_0^\infty db \int_{-\infty}^\infty db_2\, I(b_2, b_2 - b, b_l)\ , \tag{21}$$

where

$$I(b_2, b_1, b_l) = 2\,\frac{C(b_2)C(b_1)}{b} \Big\{ [1 + 3\,T\,r(x)\,\bar{\lambda}(b_2, b_1, b_l)]\,\sin(c) - \sin(b) \Big\}\ ,$$

$$c \;=\; b\,[\,1+6\,T\,\bar{\eta}(b_2,b_1,b_l)\,]\;. \tag{22}$$

5 Bethe-Heitler Limit and LPM Form Factor

To first order in $\bar{\lambda}$ and $\bar{\eta}$, each of which is proportional to the square of the net impulse given to the radiating particle, the integrand is

$$I_{\rm BH}(b_2,b_1,b_l)_1 \;=\; 6\,T\,\frac{C(b_2)C(b_1)}{b}\left\{r(x)\bar{\lambda}(b_2,b_1,b_l)\sin(b)+2\,\bar{\eta}\,(b_2,b_1,b_l)b\,\cos(b)\right\}\;. \tag{23}$$

Inserting Eq.20 for $\bar{\lambda}$ and $\bar{\eta}$, interchanging the order of the b_2 and b' integrations, and evaluating them with a suitable cutoff, yields for $(x\rightarrow 1)$

$$I(\mathrm{BH}) \;=\; 2\,\mathrm{T}\int_{-\infty}^{\infty}\mathrm{dbC(b)}\,\{3\,\mathrm{r(x)}\,\sin(\mathrm{b})+\mathrm{b}\,\cos(\mathrm{b})\} \;=\; 2\,\mathrm{T}\,[3\,\mathrm{r(x)}-1]\rightarrow 4\,\mathrm{T}\;. \tag{24}$$

This is the correct BH result in the soft photon limit. This result, as expected, does not depend upon the detailed structure or geometric arrangement of the target, only the total number of radiation lengths through the target as expressed by the integral T. In Ref.[1] a form factor F, which is unity when BH is valid, was introduced to track the LPM suppression. Here it is convenient to define

$$<I>=\; I(\mathrm{BH})\;\mathrm{F(k,T,x)}\;, \tag{25}$$

where the x dependence arises only from the spin factor $r(x)$ and T is essentially the number of mean free paths through the target. The photon momentum k together with the particle energy determine the formation length l_f. The form factor is given by

$$F(k,T,x) \;=\; \int_{-\infty}^{\infty}db\int_{-\infty}^{\infty}db_2\,F(b_2,b,b_l)\;, \tag{26}$$

where

$$F(b_2,b,b_l) \;=\; \frac{C(b)}{2\,T\,b}\left\{[1+3\,T\,r(x)\,\bar{\lambda}(b_2,b_2-b,b_l)]\,\sin(c)-\sin(b)\right\}\;,$$

$$c \;=\; b\,[\,1+6\,T\,\bar{\eta}(b_2,b_2-b,b_l)\,]\;. \tag{27}$$

6 Small k Limit

The BH limit is valid for small T and large k. The small k limit in which the formation length becomes larger than the target thickness is of interest because the suppression due to multiple scattering is manifest, yet it is not the standard LPM effect. In the limit of very small k, the effects of the index of refraction of the target medium become important; these effects are not treated here.

For small k, or large formation length l_f, the internal structure of the target becomes unimportant. The problem becomes one of radiation from a effectively thin target. In this limit one finds

$$\bar{\lambda}(b_2, b_1, b_l) \sim \theta(b_2 - B)\theta(B + b - b_2) \tag{28}$$

$$\bar{\eta}(b_2, b_1, b_l) \sim \bar{\lambda}(b_2, b_1, b_l)\,(b_2 - B)(B + b - b_2)/b^2 \ , \tag{29}$$

where B is the position of the center of the target. Writing $b_2 = B + bw$ with $db_2 = b\,dw$, allows the b integral to be performed and the form factor becomes

$$F(l_f >> l, T, 1) \sim \frac{1}{2T}\int_0^1 dw \left\{\frac{1+3T}{1+6Tw(1-w)} - 1\right\} \ , \tag{30}$$

For $T \to 0$, the form factor approaches one, the BH result. Again, this result does not depend upon the detailed structure or geometric arrangement of the target, only the integral variable T.

7 Structured Target

The cases of a thin, finite and thick homogeneous targets were discussed in Ref.[1]. From the explicit formula for the form factor F it is straightforward to carry out the integrations, at least numerically, for essentially any configuration and arrangement of the target. However the remainder of this paper will be restricted to discussing the radiation from segmented or laminated targets that are composed of identical plates

separated by a vacuum gap of constant width. The radiation length of the target plate medium will be denoted by L.

Consider a target composed of p plates each of thickness l_p and corresponding scaling variable T_p. The total target has $T = pT_p$. The gap between a pair of plates is of width l_g and there are $(p-1)$ gaps. Thus the total geometric thickness of the target is

$$l = pl_p + (p-1)l_g \ . \tag{31}$$

It is convenient to express the gap width in scaled units as well. Thus we define

$$T_g = \frac{\pi}{3}\frac{l_g}{\alpha L} \ . \tag{32}$$

The form factor will then be taken to be a function of the target variables p, T, and G, where

$$T = pT_p \qquad \text{and} \qquad G = (p-1)T_g \ . \tag{33}$$

Thus T measures the total radiation thickness of the material in the target while G measures the total thickness of the gaps. For example, a series of plots will be presented that compares the k spectrum for p and T fixed and G increasing. Of course in the BH limit of large k, F will not depend upon G. Sample numerical results will be presented in the next section.

8 Numerical Results

A macroscopic interference effect involving photons with energies in the tens of MeV will be demonstrated in the following discussion. The incident electron beam will be fixed at 25 GeV in all calculations for simplicity except for the last Figure. In order to get an order of magnitude feel for the effect consider the following. The radiation length for a gold target is $L = 3.4$mm. At a photon energy of 27MeV, the formation length

$$l_f = \frac{2xp}{m^2(1-x)} = \frac{2p_i p_f}{m^2 k} \tag{34}$$

is equal to 0.034mm, the thickness of a 1% radiator. In lead, which has $L = 5.6$mm, the formation length corresponding to a 1% radiator occurs at a lower photon energy, 16MeV. The formation length scales as the square of the incident electron energy.

In Figure 1 the small k limit of the form factor is plotted as a function of T for a target. Small T is the BH limit, whereas extremely large T is the LPM region.

The first example of a structured target to be discussed is a $T = 1$ ($\sim 0.7\%$ radiation thickness) target that is composed of two $T_p = 0.5$ laminations or plates. For this parameter set and for a gold target the formation length is equal to the original target thickness at $k = 42.4$MeV. The photon spectra is shown in Figure 2 for three values of the gap; note that $G = 1$ corresponds to a gap that is equal to the original total thickness. The photon spectrum is clearly developing a peak where the formation length is approximately equal to the distance between the centers of the plates. For smaller values of k, the form factor eventually stops decreasing and achieves the value given by Eq.30 (see Figure 1). In Figure 3 the spectrum is plotted for 5 values of the gap extending out to $G = 5$. The subsidiary peak moves down in k as the gap increases. The computed points are shown and are connected by straight lines as is the case in all the graphs.

In Figure 4 the spectra expected from a 4-segment Au target are given for several values of the gap. In this example, each plate has $T_p = 0.25$ for a total $T = 1$. The final total thickness of the target from front surface to the rear surface at $G = 9$ is ten times the original thickness while the amount of radiator material is remaining constant.

In Figure 5 the photon spectrum is given for an increasing number of plates with the total radiator thickness held again at $T = 1.0$. The gap width G is increased as the number of plates increase (and become thinner) in such a way as to hold constant the distance between the center of adjacent plates at ~ 1.5. The peak in the spectrum becomes higher and more pronounced as the number p increases and occurs at an approximately constant k value.

In Figure 6 the spectra expected from a 10-segment and a 5-segment target are plotted. The 10 plate target has a gap between each plate of $T_p = 1.4$. The 5-segment target with $T_p = 2.9$ is the same layout with every other plate removed. The shift in the peak is apparent as is some additional fine structure at higher k.

In order to get a feel for the effect of changing selected parameters consider an iron target which has $L = 17.6$mm. In Figure 7 the spectra from a 2-segment Fe target is plotted for several values of the gap at an incident energy of 50 GeV.

To demonstrate that the interference effect persists for thicker targets, the spectrum for a Au target is plotted in Figure 8 for $T = 2$ and the same energy and gap values as Figure 2. For example, at $G = 5$ the total dimensionless distance between the centers of the plates is 6. The formation length is equal to this separation at $k \sim 42.4/6 \sim 7\,\mathrm{MeV}$ which is roughly the position of the subsidiary peak.

The interference effect computed here should be straightforward to measure experimentally using the techniques pioneered in Ref.[5]. It may be possible to design structured targets to yield bremsstrahlung spectra with desirable and interesting char-

acteristics such as suppressing the soft photon part of the spectrum or enhancing the photon yield in a chosen energy regime. Finally, it is amusing that there is so much more to learn about such a well understood process.

9 Acknowledgements

I wish to thank Sid Drell, Peter Bosted, Spencer Klein, and Ralph Becker-Szendy for discussions of the LPM effect and of the data taken by the SLAC E-146 collaboration.

References

[1] R. Blankenbecler and S. D. Drell, to be published in Phys. Rev. *D* in (1996).

[2] H. A. Bethe and W. Heitler, Proc. Roy. Soc. *A146*, 83 (1934).

[3] L.D. Landau and I.J. Pomeranchuk, Dokl. Akad. Nauk. SSSR *92*, 535 (1953); *92*, 735 (1953). See also L. Landau, *The Collected Papers of L.D. Landau*, Sections 75-76, pp 586-593 Pergamon Press, (1965).

[4] A.B. Migdal, Phys. Rev. *103*, 1811 (1956).

[5] "An Accurate Measurement of the Landau, Pomeranchuk, Migdal Effect", by P. Anthony et al., SLAC-PUB-95-6796. Phys .Rev .Lett. *75*, 1949 (1995).

[6] R. Blankenbecler and S. D. Drell, Phys. Rev. *D36*, 277 (1987). An extensive list of earlier references to the eikonal method are given here.

[7] "Suppression of Radiation in an Amorphous Medium and in a Crystal", N.F. Shul'ga and S.P. Komin, JETP Lett. *27*, 117 (1978).

[8] "Theory of Emission by Relativistic Particles in Amorphous and Crystalline Media", N.V. Laskin, A.S. Mazmanishvili, N.N. Nasonov, and N.F. Shul'ga, JETP Lett. *62*, 438 (1985).

[9] "Radiation of Relativistic Particles in Single Crystals", A.I. Akhiezer, N.F. Shul'ga, Sov. Phys. Usp. *25*, 541 (1982).

[10] "Semiclassical Theory of High-Energy Particle Radiation in External Fields," A.I. Akiezer and N. F. Shul'ga, Physics Reports *234*, 297-365 (1993).

[11] R. Baier, Yu.L. Dokshitser, S. Peigne and D. Schiff, "The Landau-Pomeranchuk-Migdal Effect in QED", BI-TP 95-40, CERN-TH.96/14,CUTP-724,LPTHE-Orsay 95-84.

[12] "Notes on the Landau, Pomeranchuk, Migdal Effect: Experiment and Theory", by Martin Perl, May 1994. SLAC-PUB-6514. Presented at "Les Rencontres de Physique de la Vallee d'Aoste", La Thuile, Italy, 6-12 Mar 1994.

[13] R. Blankenbecler, "Multiple Scattering and Functional Integrals." SLAC–PUB–96–7160, (to be published).

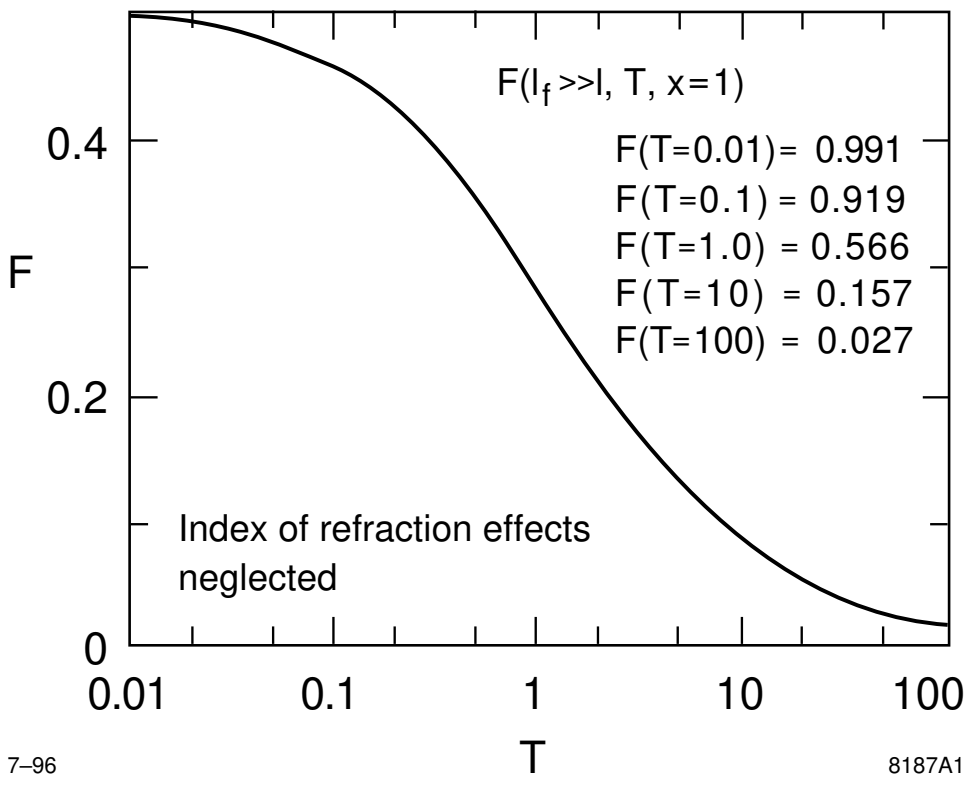

FIGURE 1
A plot of the form factor F(k,T,x) vs T for $l_f >> l$ and $x \sim 1$. The form factor is the ratio of the expected probability of emission to that predicted by Bethe-Heitler.

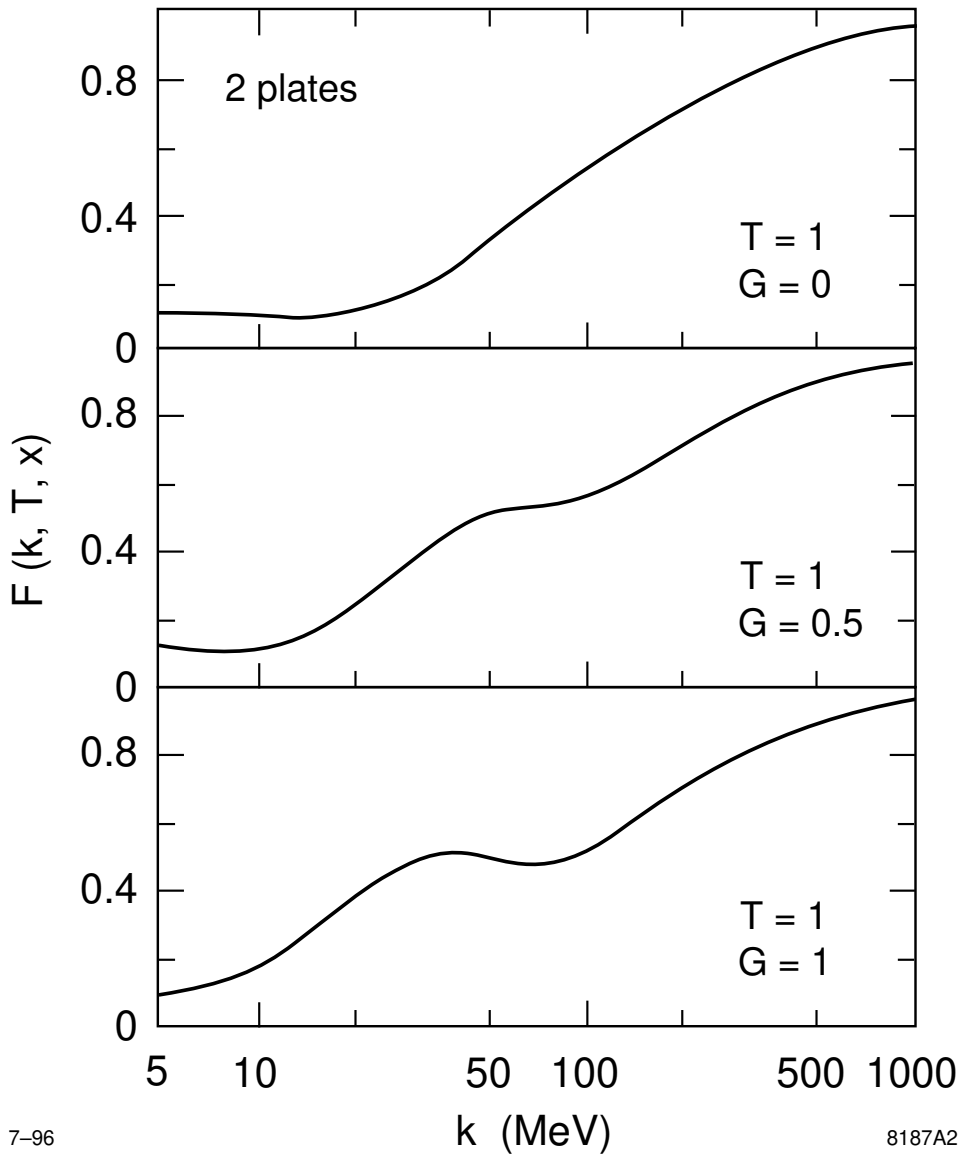

FIGURE 2
The form factor F(k,T=1,x) for a two segment Au target
for three gap values. The incident energy is 25 GeV.

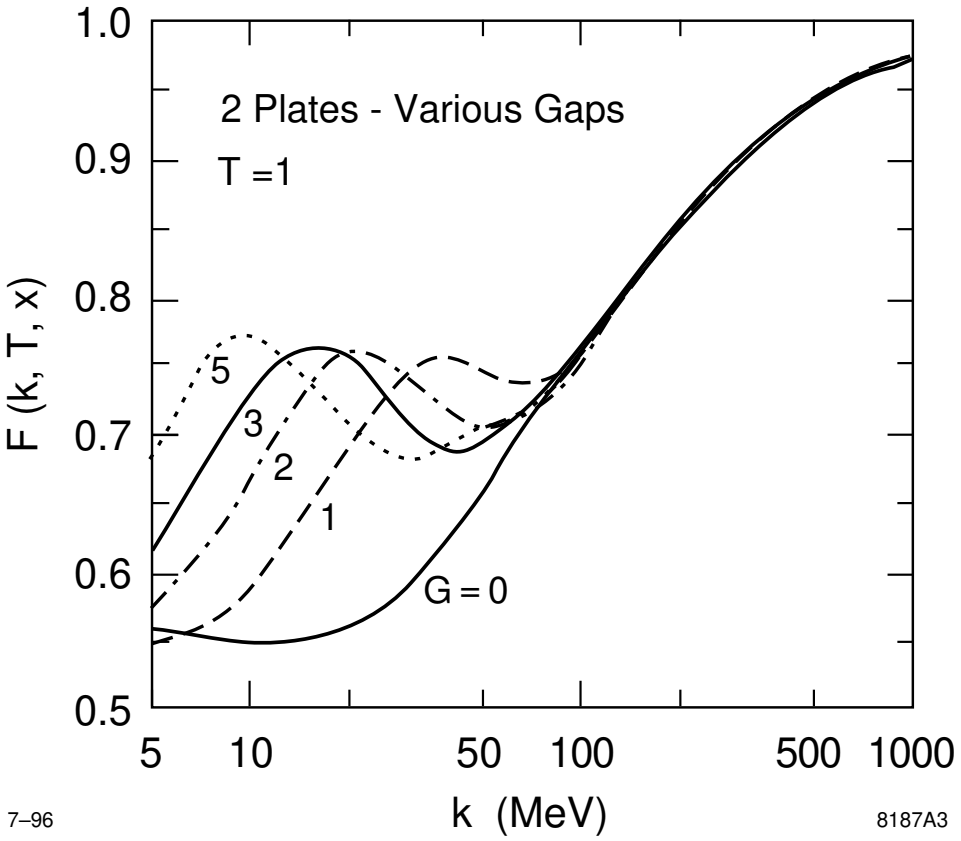

FIGURE 3
A summary graph of F(k,T=1,x) for a two segment Au target
for various gap values.

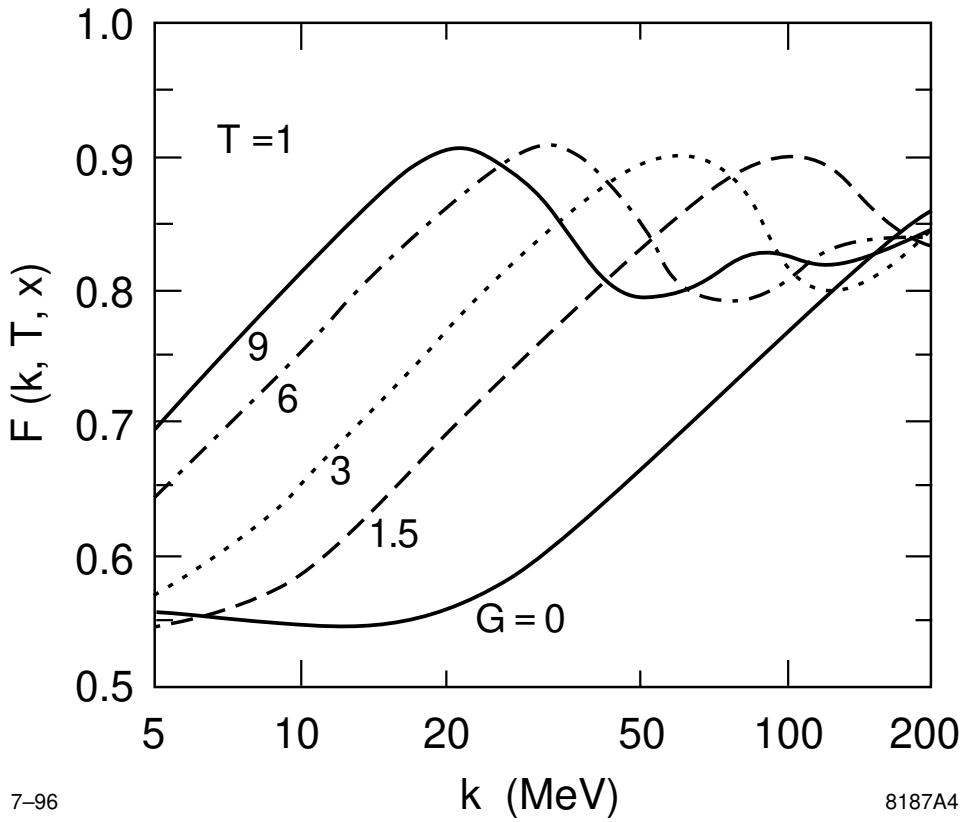

FIGURE 4
A summary graph of F(k,T=1,x) for a four segment Au target
for selected gap values.

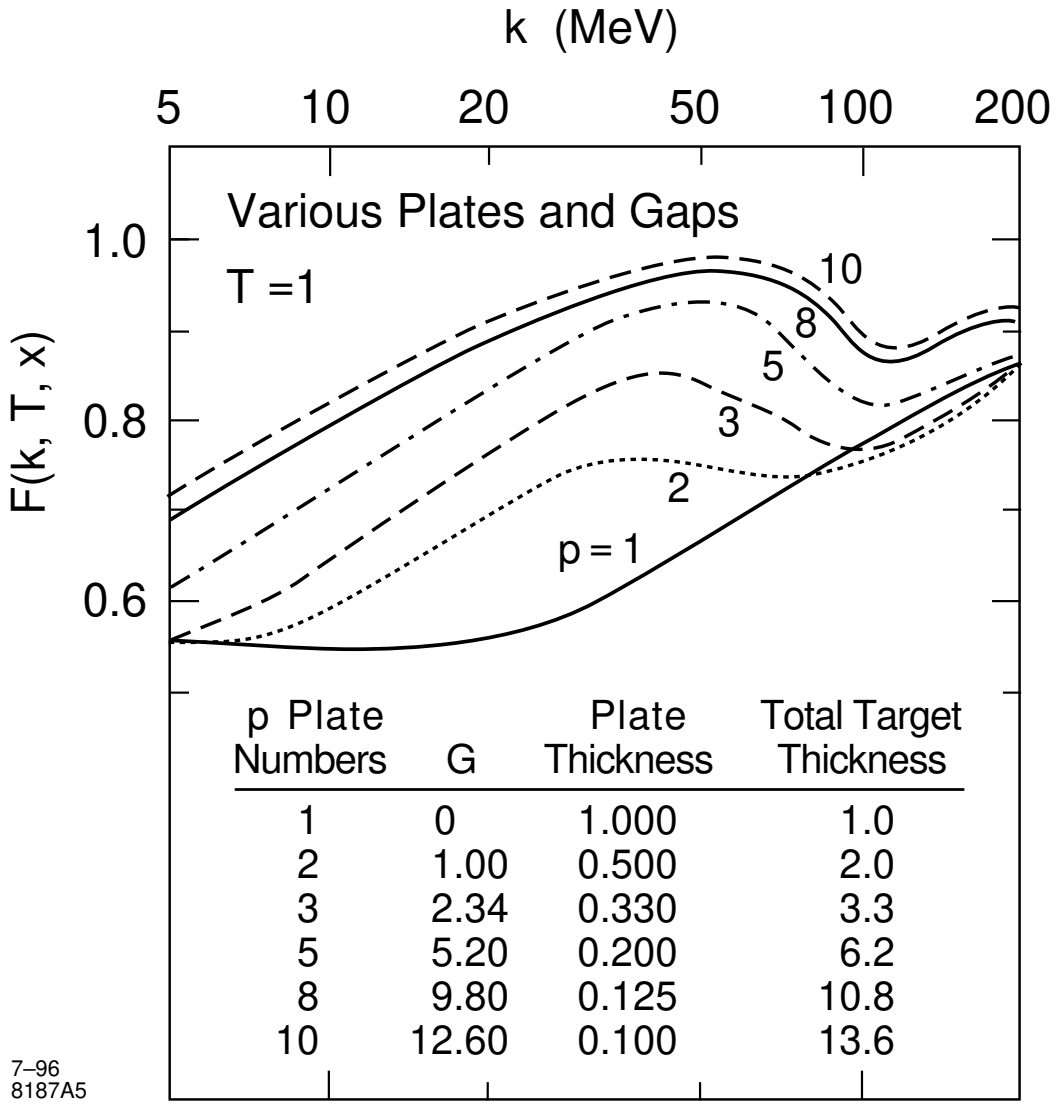

p Plate Numbers	G	Plate Thickness	Total Target Thickness
1	0	1.000	1.0
2	1.00	0.500	2.0
3	2.34	0.330	3.3
5	5.20	0.200	6.2
8	9.80	0.125	10.8
10	12.60	0.100	13.6

FIGURE 5
A summary graph of F(k,T=1,x) for a varying number of plates with differing gap values.

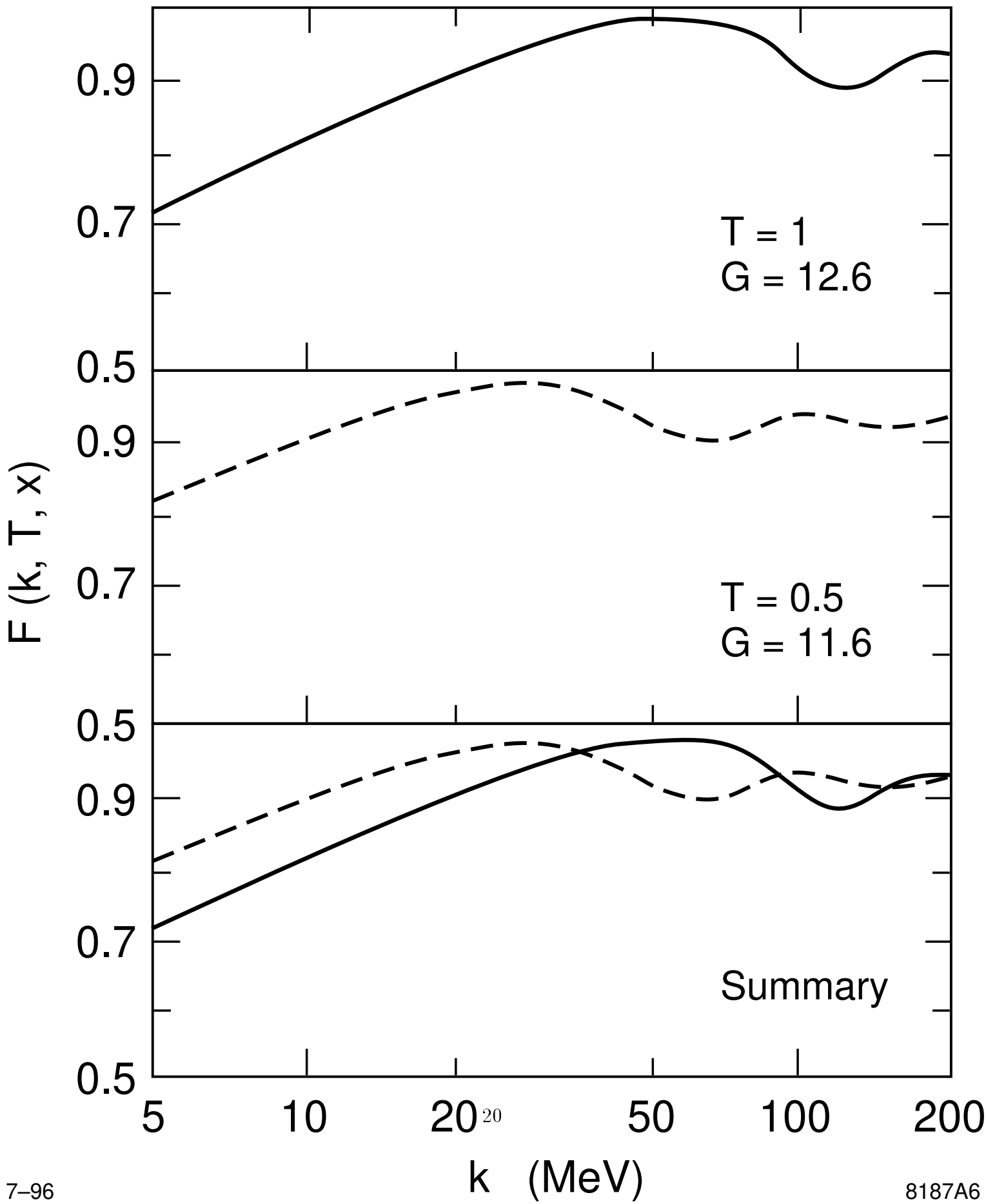
0.9
0.7
0.5
T = 1
G = 12.6
0.9
0.7
0.5
T = 0.5
G = 11.6
0.9
0.7
0.5
Summary
F (k, T, x)
5
10
20
20
50
100
200
k (MeV)

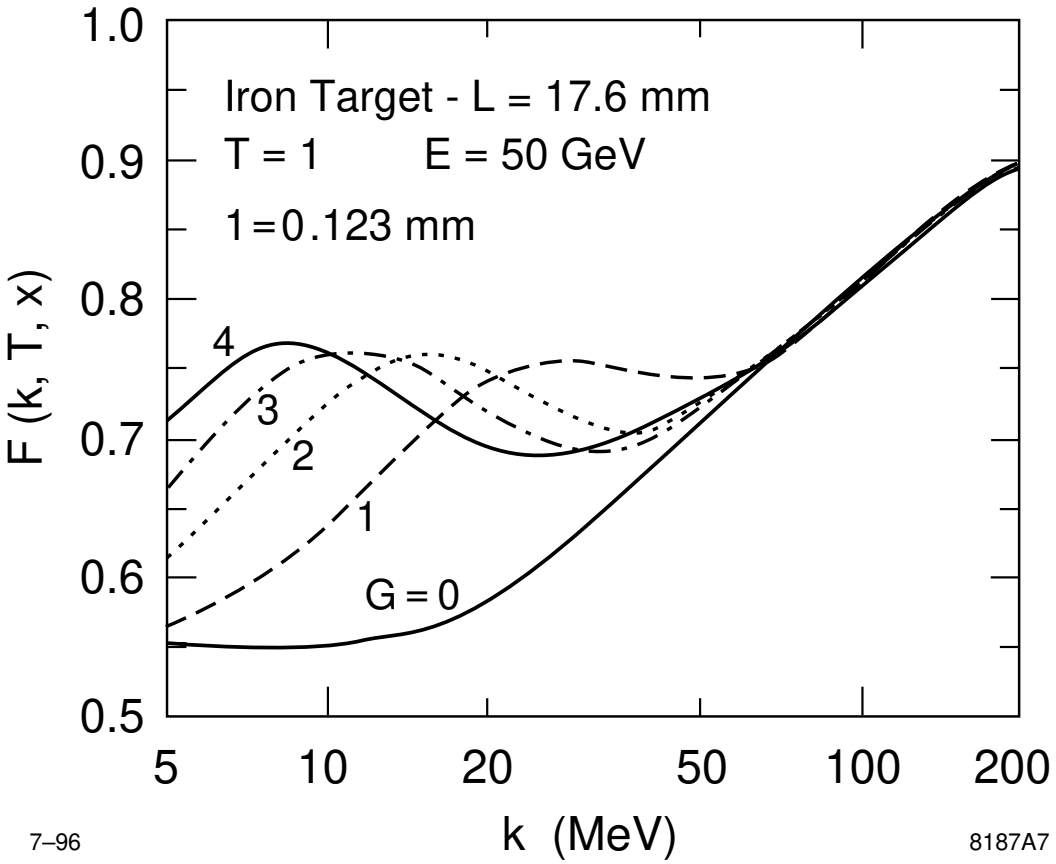

FIGURE 7
A summary graph of F(k,T=1,x) for a two segment Fe target
for various gap values at an energy of 50 GeV.

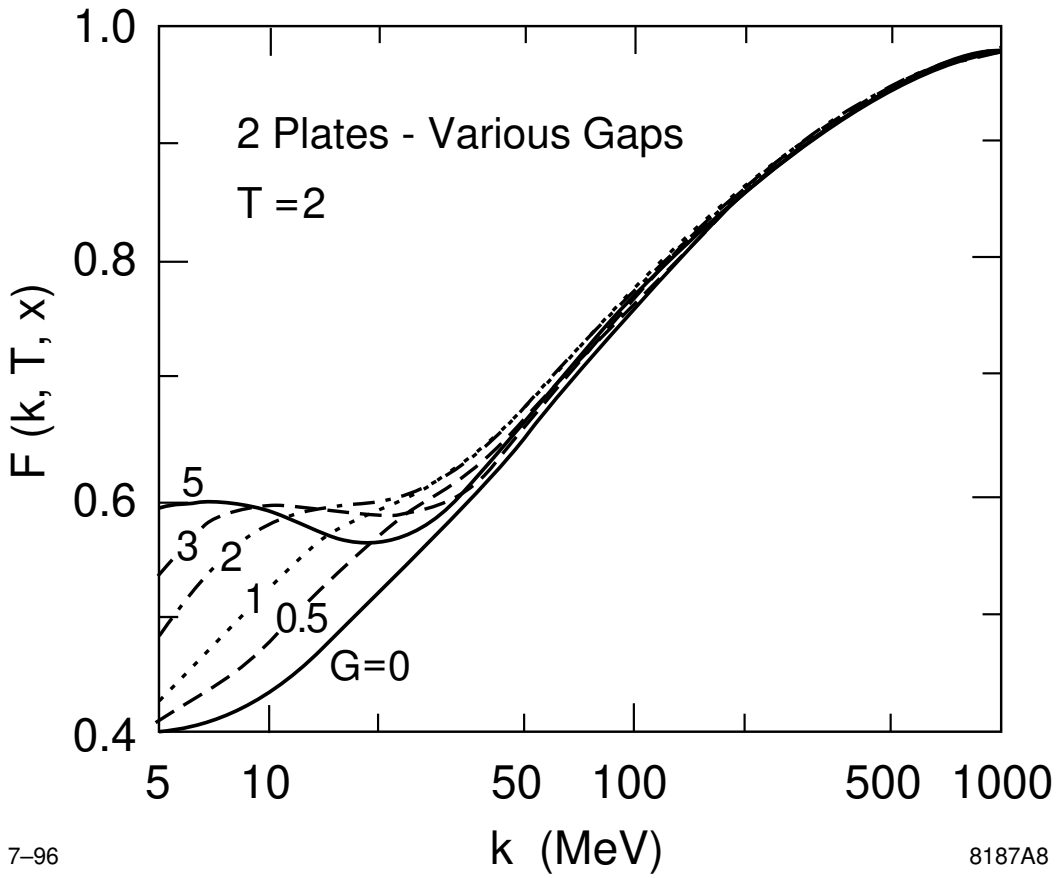

FIGURE 8
A summary graph of F(k,T=2,x) for a two segment Au target
for various gap values at an energy of 25 GeV.